Mechano–electrical transduction through anion recognition with naphthalenediimide monolayers at the air–water interface

Masaki Ishii,[*,†,‡] Yuto Nakai,[†,‡] Shion Kaneko,[†,‡] Kohei Tanaka,[‡] Yu Yamashita,[†] Kenichi Sakai,[‡] Hideki Sakai,[‡] Katsuhiko Ariga,[†,‡,¶] and Masaaki Akamatsu[*,‡,§]

†*Research Center for Materials Nanoarchitectonics (MANA), National Institute for Materials Science (NIMS), 1-1 Namiki, Tsukuba, Ibaraki 305-0044, Japan*
‡*Graduate School of Science and Technology, Tokyo University of Science, 2641 Yamazaki, Noda, Chiba 278-8510, Japan*
¶*Department of Advanced Material Science, Graduate School of Frontier Science, The University of Tokyo, 5-1-5 Kashiwanoha, Kashiwa, Chiba 277-8561, Japan*
§*Department of Chemistry and Biotechnology, Faculty of Engineering, Tottori University, Tottori, Tottori 680-8552, Japan*

E-mail: ISHII.Masaki@nims.go.jp; makamatsu@tottori-u.ac.jp

Abstract

In biological systems, various stimuli and energies are transduced into membrane potentials via ion transport or binding. The application of this concept to artificial devices may realize biomimetic signal transmitters and energy harvesters. In this study, we investigated the mechanical control of fluoride anion recognition with naphthalenediimide (NDI) monolayers at the air–water interface. Similar to the mechanosensitive ion channels in biological membranes, mechanical stimuli modulated the packing manner of the NDI monolayers, which reproducibly triggered anion binding and concomitant shifts in the membrane potential. Furthermore, mechanical stimuli resulted in anion binding or release depending on the structure of the alkyl side chains attached to the NDI molecule, which was explained by the difference in the packing manner of the NDI monolayers. These findings provide insights into the development of novel mechano–electrical transduction systems that mimic biological processes.

Introduction

Membrane potential plays a significant role in living things, for example, in generating the energy-carrying molecule ATP, sensing environmental stimuli, communicating various types of information, and performing physical motion.[1] Exploiting the membrane potential system from a biomimetic perspective is expected to fabricate a variety of high-performance artificial devices. In particular, one important proposal is energy conversion systems of mechanical stimuli, *i.e.,* kinetic energy, into electrical energy, which have attracted significant attention in recent years for energy harvesting to accelerate carbon-neutral and Internet of Things (IoT) societies.[2,3]

As shown in Fig. 1, there are several energy conversion mechanisms including the well-known piezoelectric effect, where mechanical stimuli applied to atoms with long-range order in a crystal induces polarization through relative atomic displacement.[4] In 2012, the triboelectric nanogenerator was reported, which generates a potential difference by utilizing elec-

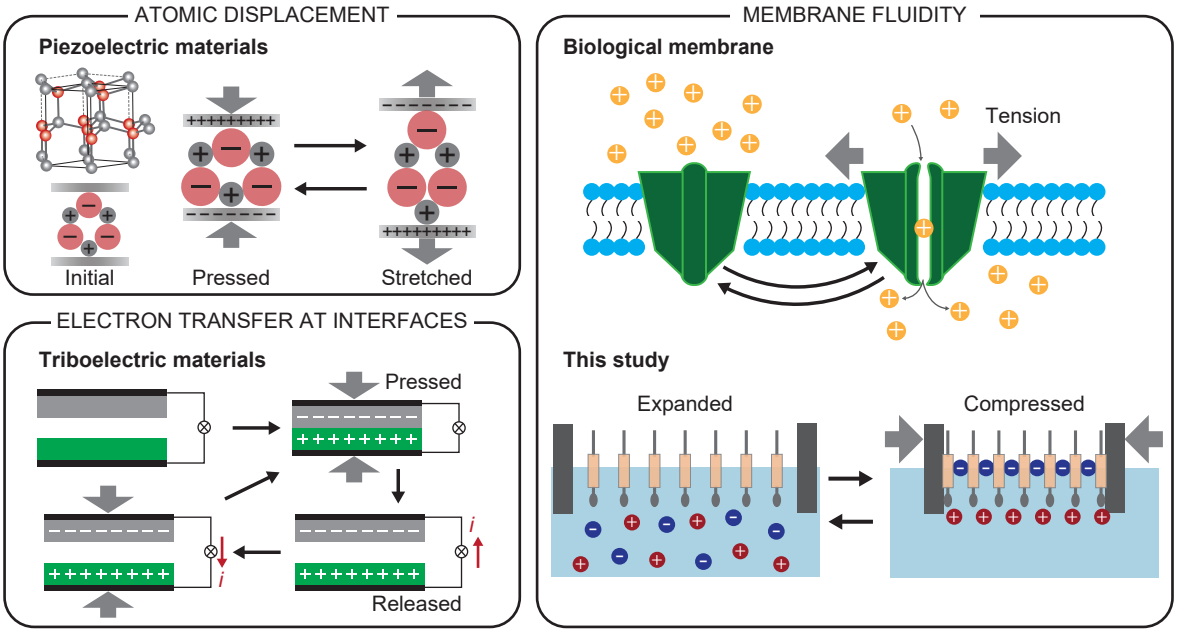

Figure 1: An overview of mechano–electrical transduction mechanisms for energy harvesting.

tron transfer induced by friction at the interface between different film materials.[5] Unlike these systems observed in solid materials, mechano–electrical transduction phenomena with a fluidity have been observed only in biological membranes. For example, Piezo1 and Piezo2 are well-known mechanosensitive ion channels[6,7] involved in many physiological functions such as light touch sensation, neuronal differentiation and erythrocyte volume regulation.[1] Hair cells in the cochlea of the inner ear also detect sound stimuli and transmit signals, which is also driven by mechanosensitive gating of ion channels.[8]

Molecular recognition and passive diffusion of ions are critical driving forces for precise control of membrane potential in biological systems. Langmuir monolayers with compositions similar to those of biological membranes have been extensively studied as suitable models for evaluating and controlling molecular recognition at the air–water interface. Many studies have investigated specific interactions between ligands and proteins, including antibodies and enzymes.[9] We have tried to finely control various molecular recognition processes using mechanical stimuli.[10–14] This was achieved by continuously adjusting the physical shape of binding sites contributing to molecular recognition, which can tune the binding constants with target species. Through such structural optimization of the binding sites, highly selective molecular recognition phenomena were demonstrated to successfully mimic the natural enzyme properties represented by the lock-and-key model. One representative research is a distinction between thymine and uracil, which differ by only one methyl group.[13] High reproducible mechano-luminescence was also realized as the example of information conversion from mechanical stimuli into change in molecular electric states through molecular recognition.[10,11]

Considering that ion motion effectively changes the membrane potential in biological systems, mechanically induced tuning of ionic recognition should be a key technique to artificially produce mechano–electrical transduction of a fluidic system. We have recently employed naphthalenediimide (NDI) derivatives[15,16] to investigate the specific interaction with anions, *i.e.*, anion–π interactions, which affect protein higher-order structure formation and enzyme reaction mechanisms.[17–19]

In this study, anion recognition in two types of NDI monolayers was controlled in response to mechanical stimuli at the air–water interface, which was quantitatively evaluated by

the charged membrane potential. The packing manner of NDI molecules dominated anion recognition, analogous to ionic channels in biological systems, indicating that different side chains functioned as determining factors for mechanically induced membrane potentials. The synthesized *n*-NDI with a saturated alkyl side chain has a high tendency to interact with each other, which facilitates molecular packing with a vertically aligned NDI core even without sufficient mechanical stimuli. The packing manner is so advantageous for anion–π interaction to prepare sandwich structure,[20,21] where the *n*-NDI monolayer is charged at a large molecular area. At the small molecular area, mechanically induced phase transition of *n*-NDI monolayer led to pushing anions out, *i.e.,* discharging. On the other hand, *iso*-NDI with a branched alkyl side chain showed the opposite trend; a low packing tendency due to the steric hindrance of the side chain offered no anion recognition at the large molecular area, although charging based on anion recognition was performed by the formation of a sandwich structure at the small molecular area. To the best of our knowledge, this is the first study to demonstrate anion binding and release with high reproducibility using a fluidic system. Therefore, this study may provide a novel platform for mechano–electrical transduction utilizing the membrane fluidity of artificial monolayers.

Results and discussion

Fundamental Analyses for Pure NDI Monolayers

The amphiphilic NDI derivatives employed in this study possess the hydrophilic part of the tetraethylene glycol group and the hydrophobic part of the alkyl groups introduced at the imide N-positions of the NDI core. In order to investigate the effects of alkyl chain structures on the phase behavior and anion recognition properties of NDIs, we synthesized *n*-NDI, *iso*-NDI, and *cis*-NDI with C8 alkyl chains that are saturated, branched, and unsaturated, respectively (Fig. 2a and see Supporting Information).

Surface pressure–molecular area (π–A) isotherms were measured to analyze fundamental monolayer characteristics, such as the two-dimensional phase and cross-sectional area of each molecule (Fig. 2b). A kink was observed at *ca.* 30 mN/m only for *n*-NDI, suggesting phase transition from phase (ii) to (iii) (the definition is described below). This phase transition phenomenon upon mechanical compression is consistent with previous results for saturated alkyl chains with carbon numbers 6 and 12.[16] Molecular cross-sectional area of *n*-NDI was estimated to be 0.36 nm^2 by extrapolating π–A curve. This value is close to the NDI core cross-sectional area of 0.31 nm^2 calculated using density functional theory (Fig. S8), suggesting that the NDI core is close-packed and nearly vertically oriented adjacent to each other in the phase (iii).

Unlike *n*-NDI with a saturated octyl group, the π–A isotherm of *iso*-NDI with a branched 2-ethylhexyl group showed no phase transition upon mechanical compression, indicating the formation of only one aggregated phase (Fig. 2b). The extrapolated value of the π–A curve was 0.45 nm^2, indicating that the steric hindrance of the branched alkyl chain prevents the dense packing of the NDI core. For *cis*-NDI with an unsaturated octenyl group, the surface pressure increased from a very small molecular area. The extrapolated value of the π–A curve was 0.22 nm^2, which is comparable to the cross-sectional area of the all-*trans* conformation of the alkyl chain (0.2 nm^2),[22,23] but much smaller than the NDI core cross-sectional area of 0.31 nm^2. This suggests that *cis*-NDI can partially dissolve in the aqueous subphase due to the unsaturated side chain with relatively high polarity (Fig. S9, 10). We concluded that detailed monolayer analysis for *cis*-NDI is difficult and worthless as well as carboxylic acids with unsaturated side chains.[24] Therefore, this study focused on the comparison between *n*-NDI and *iso*-NDI.

For further investigation, monolayers were transferred onto quartz substrates at predetermined surface pressures using the Langmuir–Blodgett (LB) technique. The UV–vis absorption spectra of the LB films are shown

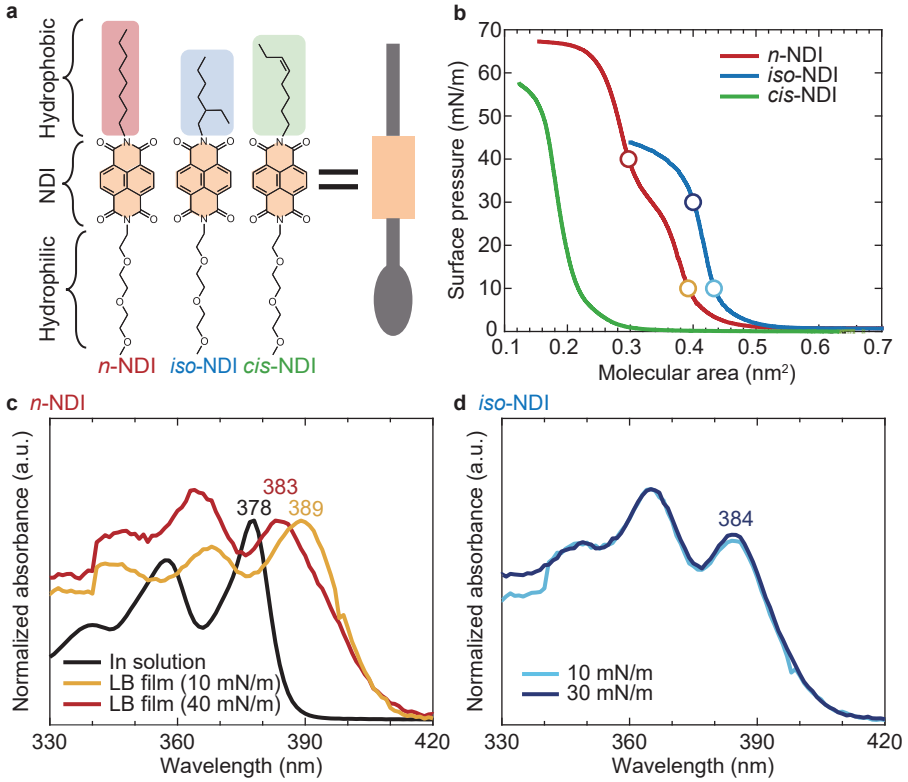

Figure 2: Assembling behavior of NDI derivatives at the air–water interface. (a) Chemical structures of NDIs with different hydrophobic moieties. (b) π–A isotherms for NDIs with indications of fixed surface pressures for transferring monolayers. (c) UV–vis spectra of *n*-NDI in acetonitrile solution (black line), in LB films transferred at 10 mN/m (orange line) and 40 mN/m (red line). (d) UV–vis spectra of *iso*-NDI in LB films transferred at 10 mN/m (light blue line) and 30 mN/m (deep blue line). Absorbance intensities are normalized against the value for a 0–0 transition around 390 nm.

in Fig. 2c, d. Similar to other types of NDI derivatives, characteristic peaks around 390 nm and 370 nm are derived from the 0–0 and 0–1 vibronic transitions of the NDI core, respectively.[21,25] For *n*-NDI, the 0–0 vibronic transition peak of LB film transferred at 10 mN/m were observed at longer wavelength of 383 nm compared to that in acetonitrile solution (378 nm), suggesting the formation of *J*-aggregates in LB films.[26,27] Further red-shifted peak was observed for *n*-NDI LB film transferred at 40 mN/m, which exceed phase transition point of 30 mN/m (Fig. 2b). This can be explained by the mechanically induced change in the molecular arrangement and orientation, *i.e.,* the packing manner, which modified the excitonic coupling[28,29] in adjacent NDI cores. However, *iso*-NDI exhibited no peak shift with increasing surface pressure, which is consistent with the absence of a kink in π–A curve of *iso*-NDI. The π–A isotherm and absorption spectra indicate that the monolayer phase and packing manner of *iso*-NDI did not change under mechanical compression. As previously confirmed with a bromine-introduced NDI derivative,[16] the introduction of bulky substituents suppresses changes in the phase of NDI monolayers upon mechanical compression. Thus, the differences in the alkyl chains allowed us to control the packing manner of the NDIs upon mechanical compression.

Anion Recognition Properties of NDI Monolayers

To evaluate the anion recognition behaviors of NDI monolayers with mechanical compression, we employed an electrolyte subphase dissolving

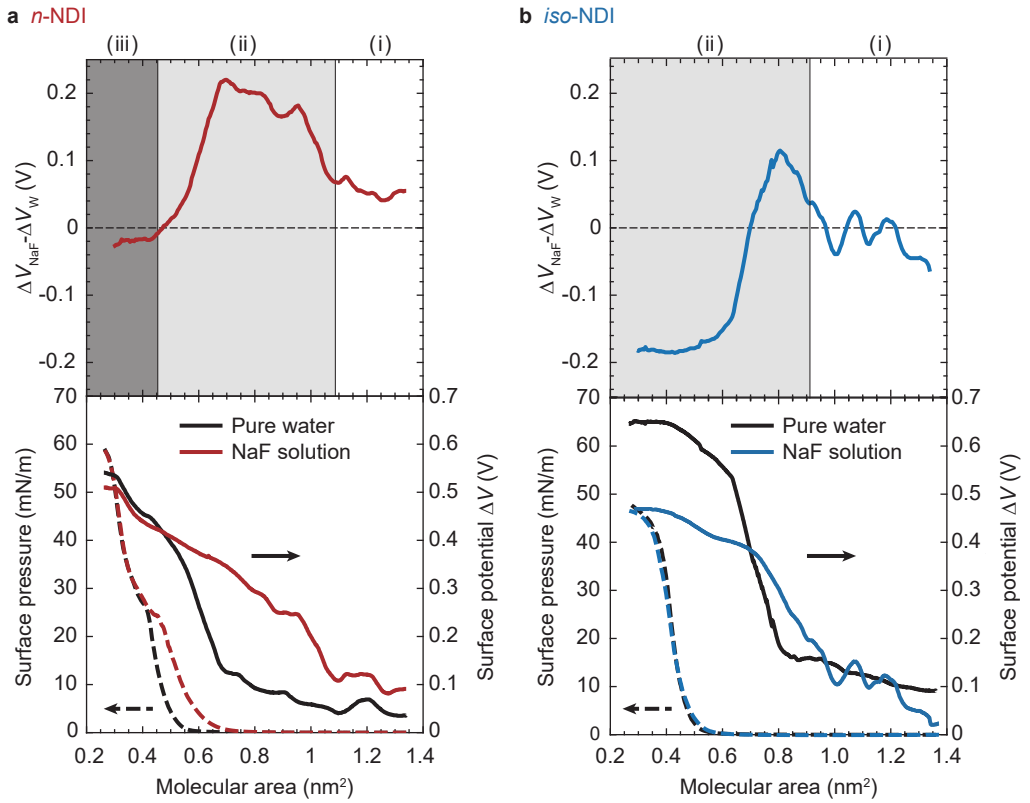

Figure 3: Surface potentials of NDI monolayers depending on anion recognition. The surface pressures and surface potentials are plotted as a function of the molecular area for (a) *n*-NDI and (b) *iso*-NDI on water with or without NaF (0.1 M). Differences in the surface potentials under the conditions of pure water and NaF solution are also shown. The surface pressure at the same molecular area differs from that in Fig. 2, which can be attributed to the effect of compression speed.[30] However, we emphasize that reproducibility under identical conditions was thoroughly confirmed.

the fluoride anion (F^-) at 0.1 M, which can be selectively sensed by NDIs rather than by direct electron transfer.[31,32] As shown in Fig. 3a, the π–A profile of *n*-NDI shifted to the larger molecular area with the addition of F^- when the surface pressure is less than phase transition point. This expansion of the *n*-NDI monolayer indicates that F^- was taken up by the monolayer driven by the anion–π interaction.[16] The increased amount in measured molecular area due to anion binding was 0.10 nm^2, approximately twice the ion cross-sectional area of 0.056 nm^2 calculated using the effective ionic radius of F^- (1.33 Å) according to Pauling.[33] This can be attributed to the efficient binding of F^- into the *n*-NDI monolayer through anion–π interaction and the electrostatic repulsion between densely bound anions. Such efficient anion binding could be due to the controlled molecular arrangement and orientation at the air–water interface, where translational and rotational motions of molecules are restricted in two dimensions, and the spontaneous molecular packing with a vertically aligned NDI core contributes to anion–π interactions to prepare the sandwich structure.[20,21] Suppressed phase transition also supported anion recognition when the surface pressure was maintained even close to critical point (Fig. S11). Note that adsorption of OH^- to the *n*-NDI monolayer can be negligible considering that pH of NaF aqueous solution was 7.89 in this study and the concentration of F^- was significantly higher by approximately five orders of magnitude than OH^- (see Supporting Information section 1.6). Interestingly, the π–A profiles of *n*-NDI with or

without NaF overlapped in the phase (iii) after the phase transition, indicating mechanically induced anion release. Furthermore, π–A isotherm of *iso*-NDI showed no change in the presence of F^-.

In-situ surface potential measurements were performed simultaneously with usual surface pressure measurement to investigate molecular arrangement and orientation[23,34] of NDIs and anion recognition property of NDI monolayers in more detail. The surface potential change (ΔV) of the Langmuir film is represented relative to the potential of pure water as follows: $\Delta V = \Delta V_p + \Phi_0$, where ΔV_p is the potential due to the permanent dipoles of the film molecules, and Φ_0 is the potential from the electric double layer. Generally, the surface potential of Langmuir films with electron-donating alkyl chains increases positively with increasing surface pressure,[23,34–36] allowing discussion on molecular density, orientation, hydration state, and interactions with chemical species in the subphase. For *n*-NDI on pure water, the surface potential began to rise at approximately 0.69 nm^2, where the surface pressure was still zero (Fig. 3a). This increase in the surface potential indicates an orientation change of *n*-NDI from a irregular and random manner to a vertically aligned one, which can be derived from island formation with no surface pressure, similar to conventional insoluble film molecules showing strong intermolecular interactions.[37,38] The slope of ΔV-A curve changed around 0.55 nm^2, where the surface pressure began to rise as the *n*-NDI molecules covered the entire water surface. For the Langmuir monolayer, the Helmholtz equation describes the relationship between the surface potential and the apparent molecular dipole moment μ_a which is modeled as a linear component: $\mu_a = \varepsilon_0 A \Delta V$, where ε_0 is the vacuum permittivity.[34,36] At molecular areas below 0.55 nm^2, apparent dipole moment of *n*-NDI continuously decreased (Fig. S12), suggesting a significant influence of mutual polarization of dipoles and rearrangement of the hydrophilic parts, commonly observed in high compression modulus films.[34,35] Therefore, the orientation in the phase (iii) of *n*-NDI using surface potential is not discussed here.

In addition to the increase in surface pressure discussed above, the comparison of surface potentials for *n*-NDI monolayer in correspondence with NaF addition into the subphase confirmed that *n*-NDI monolayer can bind F^- at a large molecular area, although it releases F^- at a small molecular area. As shown in Fig. 3a, with the addition of NaF to the subphase, the surface potential of *n*-NDI increased from molecular area of 1.07 nm^2, approximately three times the area of the close-packed structure (0.36 nm^2). At the air–water interface, the translational and rotational motion of *n*-NDI is surpassed, so that anions can synergistically promote the formation of an effective sandwich structure for anion–π interaction,[20,21] leading to an orientation change of *n*-NDI in a vertically aligned manner. Indeed, apparent dipole moment for *n*-NDI on NaF solution remained constant in the range of 0.70-0.95 nm^2 (Fig. S12), indicating almost no change in molecular orientation, while the monotonic increase in surface potential represents an only increase in molecular density. Surface potential measurement is a worthwhile way to evaluate anion-binding behavior even without changes in surface pressure. Applying sufficient mechanical compression to cause the phase transition to the phase (iii) with close-packed NDI cores led to overlapping of both the surface pressure and surface potential for the *n*-NDI monolayer on water with or without NaF, indicating the release of anions upon mechanical compression.

Interestingly, the *iso*-NDI monolayer showed an opposite trend to that of *n*-NDI in terms of the molecular area-dependent anion recognition behavior. As shown in Fig. 3b, the surface potential of *iso*-NDI monolayer was almost independent of existence of F^- in the subphase at large molecular areas above 0.96 nm^2. The surface potential increased from 0.81 nm^2 owing to the molecular orientation change on pure water, while the increase started at a slightly larger molecular area of 0.96 nm^2 in the case of adding NaF to the subphase. Similar to *n*-NDI, the contribution of the early sandwich structure formation can promote orientation change. After the apparent dipole began to decrease

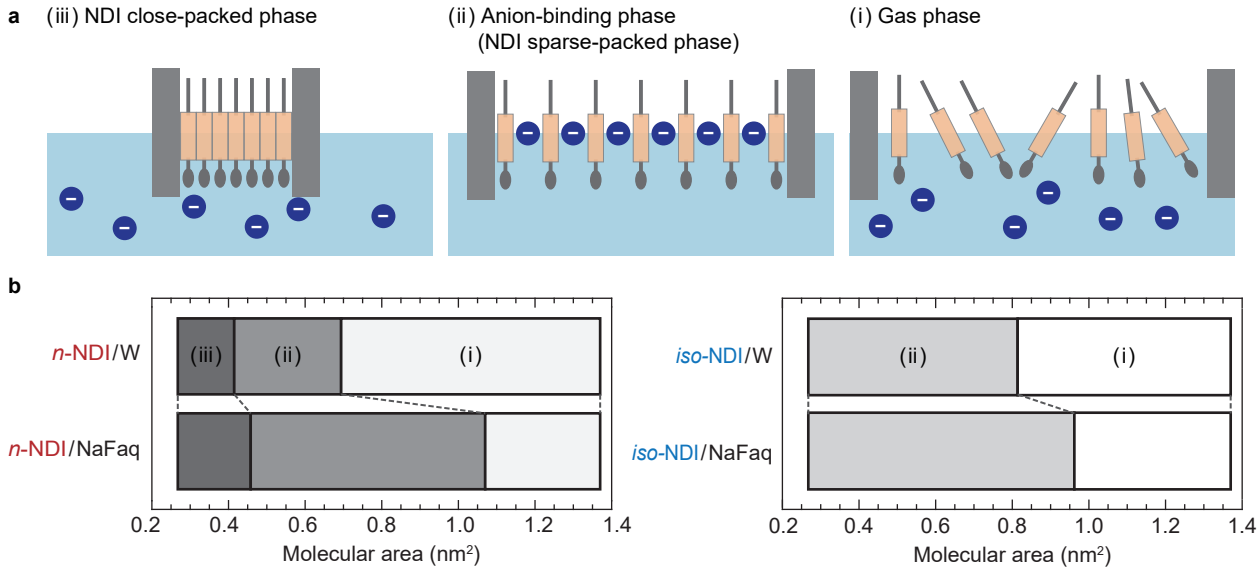

Figure 4: NDI monolayer phases at the air–water interface. (a) Schematic illustration of monolayer phases for NDIs. (i) Gas phase: NDI molecules can be mostly isolated when the surface pressure is zero and molecular area is quite large. (ii) Anion-binding (NDI sparse-packed) phase: Putting NDI molecules close to each other makes the monolayer recognize anions by sandwich structures, resulting in the more organized molecular orientation. (iii) NDI close-packed phase: a NDI monolayer pushes anions out through crystallization when a sufficient high surface pressure is applied. (b) Phase diagrams for each NDI monolayer with or without NaF at 20°C. The transition from phase (i) to phase (ii) was determined by the increase in surface potential caused by changes in molecular orientation, whereas the transition from phase (ii) to phase (iii) was determined by the kink in the π–A isotherm.

with the formation of phase (ii) at approximately 0.7 nm^2 (Fig. S12), *i.e.,* after the change in molecular orientation settled, the surface potential difference ΔV_{NaF} - ΔV_W became negative, reaching a minimum of *ca.* -0.2 V (Fig. 3b). We highlight that the negative potential difference is predominantly contributed by anion adsorption on the NDI core rather than on the ethylene glycol chain (see Supporting Information section 1.7). Furthermore, the potential difference was maintained up to the collapse pressure of the monolayer, indicating that *iso*-NDI monolayer did not release F^- upon mechanical compression. In the phase (ii), *iso*-NDI was sparsely packed because of the steric hindrance of the bulky 2-ethylhexyl alkyl chain, which created extra space between the NDI cores. Compared with the phase (iii) of *n*-NDI with close-packed NDI cores, the space can be roughly estimated as 0.09 nm^2, which is sufficient to accommodate F^- and is comparable to the increased molecular area for *n*-NDI by the addition of NaF to the subphase. Note that the similar values of the space between the NDI cores for both *n*-NDI and *iso*-NDI reasonably support the formation of sandwich structures for synergetic anion–π interaction. In addition, this scenario can explain the lack of significant changes in π–A isotherm with or without NaF in the subphase.

The abstracted phase schematics and phase diagrams are presented in Fig. 4 to overview the anion recognition behavior of NDI monolayers. At sufficiently large molecular areas, neither *n*-NDI nor *iso*-NDI interacted with anions, forming a gas phase (i) with random molecular orientation. With the mechanical compression of the monolayer, NDIs first form a sparse-packed phase or an anion-binding phase (ii) with an effective sandwich structure for anion–π interaction. The molecular area for phase transition depended on the side chains of the NDI molecules and the existence of NaF in the subphase, as summarized in Table 1. Further com-

Table 1: Critical molecular areas for the phase transition of NDI monolayers.

	n-NDI		*iso*-NDI
phase transition	(iii)–(ii)	(ii)–(i)	(ii)–(i)
Pure water	0.42 nm^2	0.69 nm^2	0.81 nm^2
NaFaq	0.46 nm^2	1.07 nm^2	0.96 nm^2

pression induced other phase transitions of the *n*-NDI monolayer to close-packed phase (iii), which was due to the low steric hindrance of the saturated alkyl chain. In this transition process, F^- bound at the *n*-NDI monolayer should be pushed out, accompanied by a change in the packing manner. On the other hand, the *iso*-NDI monolayer showed no other phase transition because of the high steric hindrance of the branched alkyl chain up to monolayer collapse. The sparse-packed structure can provide enough space between each molecule for anion accommodation driven by anion–π interaction even at small molecular areas. Therefore, the anion-binding capability and behavior of NDI monolayers can be controlled through molecular design and mechanical stimuli. Furthermore, considering our previous report that the amount of anion binding varies depending on the species and concentration of anions,[16] optimizing the molecular structure of NDI could enable the tuning of its selectivity toward specific target anions.

Repeated Anion Recognition at the Air–Water Interface

Given that molecular recognition and related properties, including mechano-luminescence in Langmuir monolayers, are reproducibly controlled by mechanical stimuli,[10,11] we demonstrated the repeated anion binding and release phenomena of identical NDI monolayers through successive compression–expansion processes. Almost equivalent profiles were acquired for each process for both surface pressure and surface potential (Fig. S13, Table S1). The moderate hysteresis indicates that NDI monolayers can bind and release F^- upon mechanical stimuli, that is, anion recognition is repeatable. Interestingly, the anion recognition behavior of each NDI monolayer showed the opposite trend, especially when compared at sufficiently small and large molecular areas. The *n*-NDI monolayer binds F^- at a large molecular area of 1 nm^2, whereas the phase transition forces it to release F^- at a small molecular area of 0.4 nm^2, which is close to the cross-sectional area of the NDI core. On the other hand, the *iso*-NDI monolayer requires greater mechanical compression for anion binding and can continue to bind F^- even at a small molecular area of 0.4 nm^2, which is due to decreased intermolecular interactions due to steric hindrance of the branched alkyl chain. Therefore, the difference in the alkyl chain structures led to opposite anion recognition behaviors through mechanical compression and expansion processes.

The surface potentials of the compression and expansion processes are shown in Fig. 5 to discuss mechano–electrical transduction phenomenon embracing reproducible anion recognition. The difference in the surface potential of the *n*-NDI monolayer depending on the presence of NaF in the subphase was obvious at 1.0 nm^2, whereas it was mainly equivalent at 0.4 nm^2. However, an obvious difference in the surface potential for the *iso*-NDI monolayer was observed only at 0.4 nm^2. As shown in Fig. 3, the amount and sign of the difference in surface potential depends on NDIs and mechanical stimuli: plus 0.2 V for expanded *n*-NDI, minus 0.2 V for compressed *iso*-NDI. Note that the value should be affected by the complex contribution of the strength and orientation of the NDI molecular dipole, the anion recognition properties of the monolayers and anion species; however, it can be optimized through molecular design and mechanical stimuli.

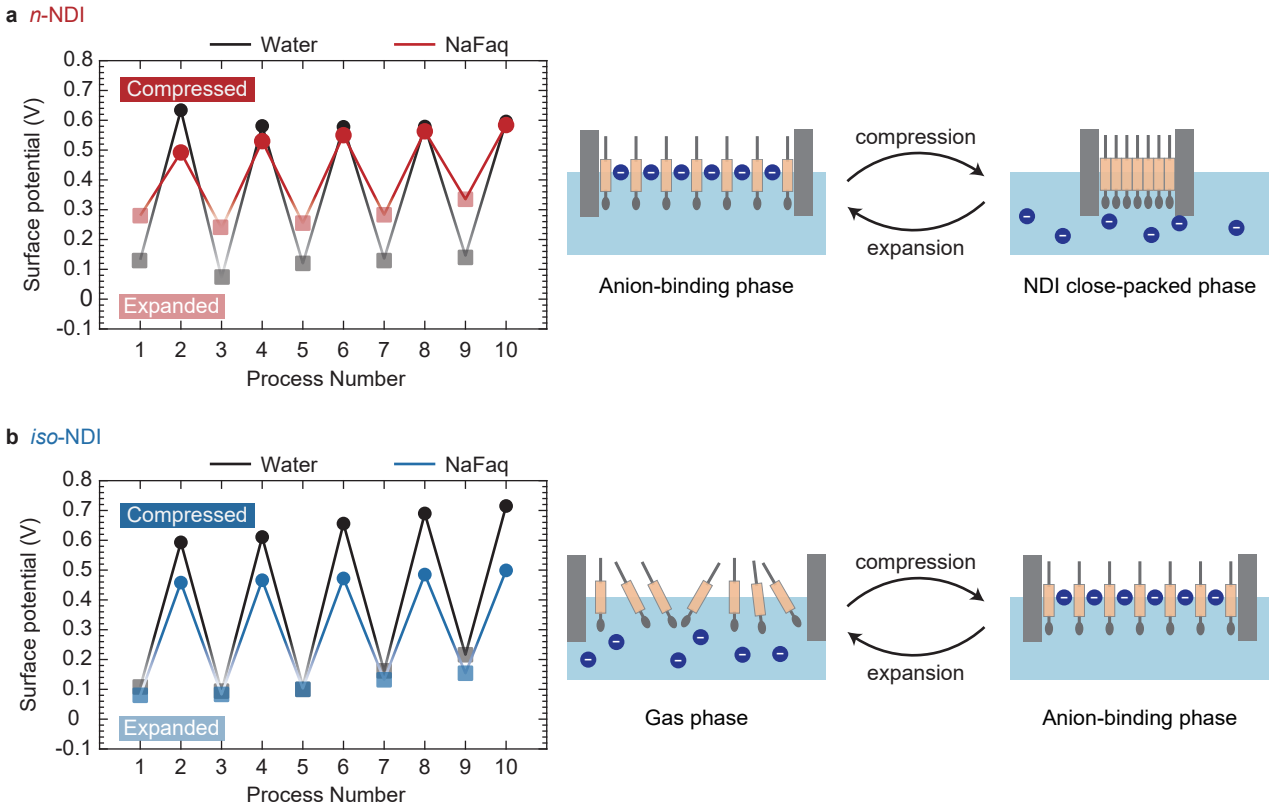

Figure 5: Repeated mechano-electrical transduction through anion recognition. Changes in the surface potential through successive compression and expansion processes are summarized for (a) *n*-NDI and (b) *iso*-NDI monolayer. Odd process numbers indicate a large molecular area of 1.0 $nm^2$and even those with a small molecular area of 0.4 nm^2. Non-zero offset of surface potentials by the existence of NaF in the subphase suggests that *n*-NDI forms anion-binding phase at large molecular area while *iso*-NDI does at small molecular area.

Inspired by the function of mechanosensitive ion channels in biological membranes, controlled generation of a difference in the surface potential of NDI monolayers was demonstrated through anion recognition. To the best of our knowledge, this is the first example of a mechano–electrical transduction phenomenon with adequate repeatability based on membrane fluidity. Our system can be applied to an actual device to produce a potential difference as the next step, similar to recent mechano–optoelectronic molecular switches.[39] A sensor for specific anions can be manufactured by optimizing the molecular structure and electron deficiency of NDI molecules. Another application may be the XOR gate in digital circuits,[40] because our system involves two types of monolayers that generate an opposite sign of a difference in surface potential under applied mechanical stimuli.

Conclusions

In this study, we demonstrated a novel approach to mechano–electrical transduction with an artificial fluidic membrane through controlled anion recognition of NDI monolayers at the air–water interface. NDI derivatives with different side chains exhibited distinct packing manners in response to mechanical stimuli, which in turn influenced anion recognition through the anion–π interaction. Specifically, *n*-NDI with saturated alkyl side chain formed three distinct two-dimensional phases: phase (i), (ii) and (iii) with increasing mechanical stimuli. Anion binding was observed exclusively in the phase (ii) formed under moderate compression; further compression led to anion

release because of the change in the packing manner. In contrast, *iso*-NDI with branched alkyl side chain formed phase (i) and (ii). Achieving anion binding through phase transition required greater compression in the *iso*-NDI monolayer than in the *n*-NDI monolayer. These findings reveal the opposite trend of anion recognition in each NDI monolayer with mechanical compression, which was quantitatively evaluated using surface potential measurements. Successive compression and expansion processes for the NDI monolayers demonstrated that the surface potential can be repeatedly modulated through precise anion recognition. The mechano–electrical transduction approach can be applied for fabricating actual devices based on a mechanically induced ion recognition monolayer.

Experimental

Materials

The solvents and reagents were purchased from Tokyo Chemical Industry Co. Ltd. (Tokyo, Japan), FUJIFILM Wako Pure Chemical (Osaka, Japan), Sigma-Aldrich Co. LLC (St. Louis, MO, US), Nacalai Tesque, Inc. (Kyoto, Japan), and GL Science Inc. (Tokyo, Japan) and used without further purification. Detailed information on the synthesis of NDI derivatives is provided in the Supporting Information.

Monolayer formation

Each NDI was dissolved in spectroscopic-grade chloroform (Dojindo Laboratories, Japan) at 0.5 mg/mL. The solution was spread onto deionized (DI) water or a NaF-containing aqueous subphase (0.1 M) in an LB trough. After 15 min of chloroform evaporation, the NDI Langmuir film was compressed to the predetermined surface pressures. Surface pressure and compression speed was calibrated using stearic acid, which is a widely utilized standard in Langmuir film studies. In the calibration step, reproducibility was confirmed under identical conditions. The temperature of the subphases was controlled at 20.0 ± 0.2°C using a chiller.

In-situ monolayer characterizations

Measurements of surface pressure–area, π–A, for Fig. 3-5 and surface potential–area, ΔV–A were performed using a Langmuir trough with a surface potential sensor (KSV NIMA). The trough contained a 150 mL subphase and had a working area of $318 \times 73 = 2.32 \times 10^4$ mm^2. The compression speed of monolayers is fixed at 0.27 mm/s.

Monolayer transfer for absorption spectroscopy

Measurements of surface pressure–area for Fig. 2 were performed and LB films were prepared on a USI-3-777C3 Langmuir–Blodgett system (USI). The trough contained a 250 mL subphase and had a working area of $334 \times 100 = 3.34 \times 10^4$ mm^2. The compression speed of monolayers is fixed at 0.20 mm/s. DI water ($> 18.2\,\Omega$ cm) was prepared using Purelab Option R7, Flex (ELGA). Compressed monolayers were transferred onto quartz by pulling the preimmersed substrate at a rate of 0.02 mm/s. The quartz substrates were treated by an ultraviolet–ozone process prior to monolayer transfer. The absorption spectra were measured using a JASCO V-670 instrument.

Acknowledgement M.I. was supported by JST, the establishment of university fellowships towards the creation of science technology innovation (Grant Number: JPMJFS2144). This work was also supported by KAKENHI (Grant Numbers: JP20H00392 and JP23H05459), the Foundation Oil & Fat Industry Kaikan, and the Foundation for the Promotion of Ion Engineering. We are grateful to Prof. Takeshi Kondo and Dr. Toshifumi Tojo for supporting the surface-potential measurements.

Supporting Information Available

The Supporting Information is available free of charge at

- Experimental details, synthetic procedures, characterization data, additional π–A isotherms, UV–vis absorption spectra, and DFT calculations (PDF)

References

(1) Wu, J.; Lewis, A. H.; Grandl, J. Touch, tension, and transduction–the function and regulation of Piezo ion channels. *Trends in biochemical sciences* **2017**, *42*, 57–71.

(2) Vijayakanth, T.; Shankar, S.; Finkelstein-Zuta, G.; Rencus-Lazar, S.; Gilead, S.; Gazit, E. Perspectives on recent advancements in energy harvesting, sensing and bio-medical applications of piezoelectric

gels. *Chemical Society Reviews* **2023**, *52*, 6191–6220.

(3) Chen, K.; Ho, D. Piezoionics: Mechanical-to-ionic transduction for sensing, biointerface, and energy harvesting. *Aggregate* **2024**, *5*, e425.

(4) Anton, S. R.; Sodano, H. A. A review of power harvesting using piezoelectric materials (2003–2006). *Smart materials and Structures* **2007**, *16*, R1.

(5) Fan, F.-R.; Tian, Z.-Q.; Wang, Z. L. Flexible triboelectric generator. *Nano energy* **2012**, *1*, 328–334.

(6) Coste, B.; Mathur, J.; Schmidt, M.; Earley, T. J.; Ranade, S.; Petrus, M. J.; Dubin, A. E.; Patapoutian, A. Piezo1 and Piezo2 are essential components of distinct mechanically activated cation channels. *Science* **2010**, *330*, 55–60.

(7) Zhao, Q.; Zhou, H.; Chi, S.; Wang, Y.; Wang, J.; Geng, J.; Wu, K.; Liu, W.; Zhang, T.; Dong, M.-Q.; Wang, J.; Li, X.; Xiao, B. Structure and mechanogating mechanism of the Piezo1 channel. *Nature* **2018**, *554*, 487–492.

(8) Liu, S.; Wang, S.; Zou, L.; Xiong, W. Mechanisms in cochlear hair cell mechano-electrical transduction for acquisition of sound frequency and intensity. *Cellular and Molecular Life Sciences* **2021**, *78*, 5083–5094.

(9) Ahlers, M.; Müller, W.; Reichert, A.; Ringsdorf, H.; Venzmer, J. Specific interactions of proteins with functional lipid monolayers—ways of simulating biomembrane processes. *Angewandte Chemie International Edition in English* **1990**, *29*, 1269–1285.

(10) Ariga, K.; Terasaka, Y.; Sakai, D.; Tsuji, H.; Kikuchi, J.-i. Piezoluminescence based on molecular recognition by dynamic cavity array of steroid cyclophanes at the air- water interface. *Journal of the American Chemical Society* **2000**, *122*, 7835–7836.

(11) Ariga, K.; Nakanishi, T.; Terasaka, Y.; Tsuji, H.; Sakai, D.; Kikuchi, J.-i. Piezoluminescence at the air- water interface through dynamic molecular recognition driven by lateral pressure application. *Langmuir* **2005**, *21*, 976–981.

(12) Michinobu, T.; Shinoda, S.; Nakanishi, T.; Hill, J. P.; Fujii, K.; Player, T. N.; Tsukube, H.; Ariga, K. Mechanical control of enantioselectivity of amino acid recognition by cholesterol-armed cyclen monolayer at the air-water interface. *Journal of the American Chemical Society* **2006**, *128*, 14478–14479.

(13) Mori, T.; Okamoto, K.; Endo, H.; Hill, J. P.; Shinoda, S.; Matsukura, M.; Tsukube, H.; Suzuki, Y.; Kanekiyo, Y.; Ariga, K. Mechanical tuning of molecular recognition to discriminate the single-methyl-group difference between thymine and uracil. *Journal of the American Chemical Society* **2010**, *132*, 12868–12870.

(14) Sakakibara, K.; Joyce, L. A.; Mori, T.; Fujisawa, T.; Shabbir, S. H.; Hill, J. P.; Anslyn, E. V.; Ariga, K. A mechanically controlled indicator displacement assay. *Angewandte Chemie International Edition* **2012**, *38*, 9643–9646.

(15) Akamatsu, M.; Kimura, A.; Yamanaga, K.; Sakai, K.; Sakai, H. Anion–π interaction at the solid/water interfaces. *Chemical Communications* **2021**, *57*, 4650–4653.

(16) Akamatsu, M.; Yamanaga, K.; Tanaka, K.; Kanehara, Y.; Sumita, M.; Sakai, K.; Sakai, H. Anion- π Interactions in Monolayers Formed by Amphiphilic Electron-Deficient Aromatic Compounds at Air/Water Interfaces. *Langmuir* **2023**, *39*, 5833–5839.

(17) Chifotides, H. T.; Dunbar, K. R. Anion-π interactions in supramolecular architectures. *Accounts of chemical research* **2013**, *46*, 894–906.

(18) Giese, M.; Albrecht, M.; Rissanen, K. Anion- π interactions with fluoroarenes. *Chemical Reviews* **2015**, *115*, 8867–8895.

(19) Zhao, Y.; Cotelle, Y.; Liu, L.; López-Andarias, J.; Bornhof, A.-B.; Akamatsu, M.; Sakai, N.; Matile, S. The emergence of anion- π catalysis. *Accounts of chemical research* **2018**, *51*, 2255–2263.

(20) Rananaware, A.; Samanta, M.; Bhosale, R. S.; Kobaisi, M. A.; Roy, B.; Bheemireddy, V.; Bhosale, S. V.; Bandyopadhyay, S.; Bhosale, S. V. Photomodulation of fluoride ion binding through anion-π interactions using a photoswitchable azobenzene system. *Scientific Reports* **2016**, *6*, 22928.

(21) Bornhof, A.-B.; Bauzá, A.; Aster, A.; Pupier, M.; Frontera, A.; Vauthey, E.; Sakai, N.; Matile, S. Synergistic Anion–(π) n–π Catalysis on π-Stacked Foldamers. *Journal of the American Chemical Society* **2018**, *140*, 4884–4892.

(22) Kaganer, V. M.; Möhwald, H.; Dutta, P. Structure and phase transitions in Langmuir monolayers. *Reviews of Modern Physics* **1999**, *71*, 779.

(23) Oliveira Jr, O. N.; Bonardi, C. The surface potential of Langmuir monolayers revisited. *Langmuir* **1997**, *13*, 5920–5924.

(24) Tomoaia-Cotişel, M.; Zsako, J.; Mocanu, A.; Lupea, M.; Chifu, E. Insoluble mixed monolayers: III. The ionization characteristics of some fatty acids at the air/water interface. *Journal of colloid and interface science* **1987**, *117*, 464–476.

(25) Barros, T. C.; Brochsztain, S.; Toscano, V. G.; Berci Filho, P.; Politi, M. J. Photophysical characterization of a 1, 4, 5, 8-naphthalenediimide derivative. *Journal of Photochemistry and Photobiology A: Chemistry* **1997**, *111*, 97–104.

(26) Jones, B. A.; Facchetti, A.; Wasielewski, M. R.; Marks, T. J. Effects of arylene diimide thin film growth conditions on n-channel OFET performance. *Advanced Functional Materials* **2008**, *18*, 1329–1339.

(27) Shao, H.; Nguyen, T.; Romano, N. C.; Modarelli, D. A.; Parquette, J. R. Self-assembly of 1-D n-type nanostructures based on naphthalene diimide-appended dipeptides. *Journal of the American Chemical Society* **2009**, *131*, 16374–16376.

(28) Ishii, M.; Mori, T.; Nakanishi, W.; Hill, J. P.; Sakai, H.; Ariga, K. Helicity manipulation of a double-paddled binaphthyl in a two-dimensional matrix field at the air–water interface. *ACS nano* **2020**, *14*, 13294–13303.

(29) Ishii, M.; Mori, T.; Nakanishi, W.; Hill, J. P.; Sakai, H.; Ariga, K. Mechanical tuning of aggregated states for conformation control of cyclized binaphthyl at the air–water interface. *Langmuir* **2022**, *38*, 6481–6490.

(30) Gourier, C.; Knobler, C. M.; Daillant, J.; Chatenay, D. Collapse of monolayers of 10, 12-pentacosadiyonic acid: kinetics and structure. *Langmuir* **2002**, *18*, 9434–9440.

(31) Bélanger-Chabot, G.; Ali, A.; Gabbaï, F. P. On the reaction of naphthalene diimides with fluoride ions: Acid/base versus redox reactions. *Angewandte Chemie International Edition* **2017**, *56*, 9958–9961.

(32) Tam, T. L. D.; Xu, J. W. The role of fluoride in anion–π interaction with naphthalene diimide. *Chemical Communications* **2019**, *55*, 6225–6228.

(33) Pauling, L. *The nature of the chemical bond and the structure of molecules and*

crystals: an introduction to modern structural chemistry; Cornell university press, 1960; Vol. 18.

(34) Oliveira, O. N.; Taylor, D. M.; Lewis, T. J.; Salvagno, S.; Stirling, C. J. Estimation of group dipole moments from surface potential measurements on Langmuir monolayers. *Journal of the Chemical Society, Faraday Transactions 1: Physical Chemistry in Condensed Phases* **1989**, *85*, 1009–1018.

(35) Paltauf, F.; Hauser, H.; Phillips, M. Monolayer characteristics of some 1, 2-diacyl, 1-alkyl-2-acyl and 1, 2-dialkyl phospholipids at the air-water interface. *Biochimica et Biophysica Acta (BBA)-Biomembranes* **1971**, *249*, 539–547.

(36) Jurak, M.; Szafran, K.; Cea, P.; Martín, S. Analysis of molecular interactions between components in phospholipid-immunosuppressant-antioxidant mixed Langmuir films. *Langmuir* **2021**, *37*, 5601–5616.

(37) Seoane, R.; Minones, J.; Conde, O.; Miñones, J.; Casas, M.; Iribarnegaray, E. Thermodynamic and Brewster angle microscopy studies of fatty acid/cholesterol mixtures at the air/water interface. *The Journal of Physical Chemistry B* **2000**, *104*, 7735–7744.

(38) Li, C.; Zhao, B.; Lu, Y.; Liang, Y. Microstructure and ion exchange in stearic acid Langmuir–Blodgett films studied by Fourier transform infrared-attenuated total reflection spectroscopy. *Journal of Colloid and Interface science* **2001**, *235*, 59–65.

(39) Yang, Z.; Cazade, P.-A.; Lin, J.-L.; Cao, Z.; Chen, N.; Zhang, D.; Duan, L.; Nijhuis, C. A.; Thompson, D.; Li, Y. High performance mechano-optoelectronic molecular switch. *Nature communications* **2023**, *14*, 5639.

(40) Erbas-Cakmak, S.; Kolemen, S.; Sedgwick, A. C.; Gunnlaugsson, T.; James, T. D.; Yoon, J.; Akkaya, E. U. Molecular logic gates: the past, present and future. *Chemical Society Reviews* **2018**, *47*, 2228–2248.

TOC Graphic

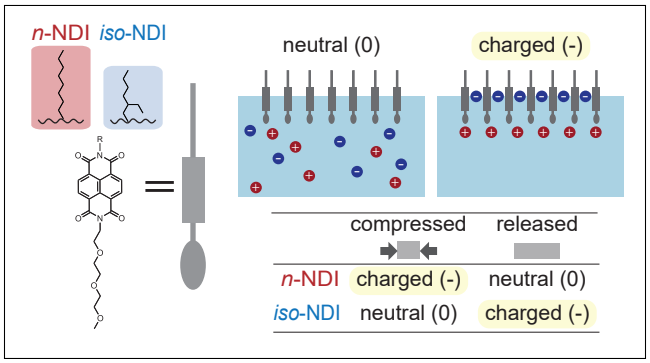
n-NDI
iso-NDI
neutral (0)
charged (-)
compressed
released
n-NDI
charged (-)
neutral (0)
iso-NDI
neutral (0)
charged (-)